Remote Sens. **2014**, *6*, 4369-4390; doi:10.3390/rs6054369

OPEN ACCESS

remote sensing

ISSN 2072-4292

www.mdpi.com/journal/remotesensing

Article

Daily Evaporative Fraction Parameterization Scheme Driven by Day–Night Differences in Surface Parameters: Improvement and Validation

Jing Lu [1,2], Ronglin Tang [1], Huajun Tang [3,*], Zhao-Liang Li [3,4], Guoqing Zhou [5], Kun Shao [6], Yuyun Bi [3] and Jelila Labed [4]

1 State Key Laboratory of Resources and Environmental Information System, Institute of Geographic Sciences and Natural Resources Research, Chinese Academy of Sciences, Beijing 100101, China; E-Mails: lujingljx@126.com (J.L.); trl_wd@163.com (R.T.)

2 University of Chinese Academy of Sciences, Beijing 100049, China

3 Key Laboratory of Agri-Informatics, Ministry of Agriculture/Institute of Agricultural Resources and Regional Planning, Chinese Academy of Agricultural Sciences, Beijing 100081, China; E-Mails: lizhaoliang@caas.cn (Z.-L.L.);biyuyun@caas.cn (Y.B.)

4 ICube, UdS, CNRS, 300 Bld Sebastien Brant, CS10413, Illkirch F-67412, France; E-Mail: labed@unistra.fr

5 Guangxi Key Laboratory of Saptial Information and Geomatics, Guilin University of Technology, Guangxi 541004, China; E-Mail: gzhou@glut.edu.cn

6 School of Computer and Information, HeFei University of Technology, Hefei 230009, China; E-Mail: shaokun@hfut.edu.cn

***** Author to whom correspondence should be addressed; E-Mail: hjtang@caas.cn; Tel.: +86-10-8210-9395.

Received: 31 March 2014; in revised form: 29 April 2014 / Accepted: 4 May 2014 / Published: 12 May 2014

Abstract: In a previous study, a daily evaporative fraction (EF) parameterization scheme was derived based on day–night differences in surface temperature, air temperature, and net radiation. Considering the advantage that incoming solar radiation can be readily retrieved from remotely sensed data in comparison with surface net radiation, this study simplified the daily EF parameterization scheme using incoming solar radiation as an input. Daily EF estimates from the simplified scheme were nearly equivalent to the results from the original scheme. *In situ* measurements from six Ameriflux sites with different land covers were used to validate the new simplified EF parameterization scheme. Results showed that daily EF estimates for clear skies were consistent with the *in situ* EF corrected

by the residual energy method, showing a coefficient of determination of 0.586 and a root mean square error of 0.152. Similar results were also obtained for partly clear sky conditions. The non-closure of the measured energy and heat fluxes and the uncertainty in determining fractional vegetation cover were likely to cause discrepancies in estimated daily EF and measured counterparts. The daily EF estimates of different land covers indicate that the constant coefficients in the simplified EF parameterization scheme are not strongly site-specific.

Keywords: evaporative fraction; day–night differences; validation; Ameriflux sites

1. Introduction

Studies on surface energy and water budgets require accurate evapotranspiration (ET) information at large spatial scales [1,2]. Satellite-based data can be used for the ET estimation [3,4]. Physical ET models based on remotely sensed data (e.g., one-source models and two-source models [5–11]) require ground-based measurements. This hinders the application of these models particularly to ungauged areas with few ground-based measurements. Therefore, it is advantageous to develop ET models that completely depend on surface parameters/variables retrieved from remote sensing. Surface parameters/variables that can be extracted from remotely sensed data mainly include surface temperature, surface emissivity, albedo, vegetation indices, leaf area index, soil moisture, net radiation, solar radiation, and air temperature [12–22]. Some simple methods can estimate surface energy fluxes by directly using these remotely sensed surface parameters/variables (e.g., empirical equations and the triangle feature space [23–28]). However, the dependence of site and spatial domain is the main disadvantage of these methods [29,30]. In addition, these methods are mainly driven by remotely sensed surface variables from a one-time observation.

The temporal variation in remotely sensed parameters/variables contains important information on surface fluxes, and it has been shown to be insensitive to retrieval error from remote sensing [31–37]. Based on surface energy balance, the bulk heat transfer equation for sensible heat flux, and the assumption of fairly invariant evaporative fraction (EF) during the daytime, Lu *et al.* (2013) [38] derived a new parameterization scheme of directly estimating daily EF, which is parameterized as a function of temporal variations in surface temperature, air temperature, and net radiation. The input requirements can be easily met by remotely sensed data from the MODIS sensor and sensors onboard geostationary meteorological satellites. The parameterization scheme was applied to the Yucheng station in North China and encouraging results were obtained. Considering the relatively easy estimation of incoming solar radiation from remotely sensed data, this study will simplify the daily EF parameterization scheme using incoming solar radiation as an input. Details about the simplification will be presented in Section 2. To further clarify the potential ability of the simplified EF parameterization scheme and examine whether it is site-specific, ground-based measurements from Ameriflux sites with different vegetation types will be used to validate the EF estimates. Data and processing will be described in Section 3. Results and the uncertainties for EF estimates are analyzed in Section 4, and summaries and conclusions will be provided in Section 5.

2. Method

On the basis of the surface energy balance equation, surface latent heat flux (*LE*) at any time *t* in a day is expressed as follows:

$$LE(t) = R_n(t) - G(t) - H(t) = Q(t) - H(t) \quad (1)$$

where R_n is the net radiation, G is the soil heat flux, H is the sensible heat flux, and Q is the surface available energy, which is equal to $R_n - G$ and all variables are expressed in units of W/m^2.

The derivative of Equation (1) with respect to t is written as follows:

$$\frac{dLE}{dt} = \frac{dQ}{dt} - \frac{dH}{dt} \quad (2)$$

H is theoretically determined by aerodynamic temperature (T_{aero}). Because T_{aero} is not easily measured, surface radiative temperature (T_s) is frequently used to replace T_{aero} for H estimates. By defining radiometric heat conductance (P_{rad}) corresponding to T_s [39,40], H is expressed as follows:

$$H = P_{rad}(T_s - T_a) \quad (3)$$

where T_a is the air temperature (K). During a short study period of dt, provided that P_{rad} depending on atmosphere and surface properties does not change considerably, the variation of H with time t is written as follows:

$$\frac{dH}{dt} = P_{rad}\left(\frac{dT_s}{dt} - \frac{dT_a}{dt}\right) \quad (4)$$

Combining Equations (2) and (4), the following equation is derived:

$$\frac{dLE}{dt} \Big/ \frac{dQ}{dt} = 1 - \frac{dH}{dt} \Big/ \frac{dQ}{dt} = 1 - P_{rad}\left(\frac{dT_s}{dt} - \frac{dT_a}{dt}\right) \Big/ \frac{dQ}{dt} \quad (5)$$

From a study by Carlson *et al.* (1995) [23], P_{rad} almost linearly varies with fractional vegetation coverage (f_c). G is frequently assumed to be proportional to R_n, depending on f_c [5]. On the basis of the assumptions of relatively invariant EF during the daytime and low evaporation at night [41,42], daily average EF can be substituted by an instantaneous EF during the daytime. As a result, daily EF is parameterized as [38]:

$$EF_{daily} = EF(t) = \frac{dLE}{dt} \Big/ \frac{dQ}{dt} = 1 - (A \times f_c^{\,2} + B \times f_c + C)\left(\frac{dT_s}{dt} - \frac{dT_a}{dt}\right) \Big/ \frac{dR_n}{dt} \quad (6)$$

The variable dt in above equations is not required for a long period. It is generally universal that T_s, T_a, and R_n on cloud-free days vary linearly with time during the morning [31,33]. Therefore, the slope of the linear relationship can be used in Equation (6). Additionally, the day–night differences in T_s, T_a, and R_n can be also applied because the day–night differences in surface parameters are almost positively proportioned to their variations during the morning, *i.e.*,

$$EF_{daily} = 1 - (A \times f_c^{\,2} + B \times f_c + C)\frac{\Delta T_s - \Delta T_a}{\Delta R_n} \quad (7)$$

where ΔT_s, ΔT_a, and ΔR_n are the day–night differences in T_s, T_a, and R_n or their variation during the morning. Considering the application for remotely sensed data from a geostationary meteorological

satellite or a polar orbit satellite with a MODIS sensor, inputs for equation (7) are based on five different schemes including (1) change rate during the morning, (2) differences between 1:30 P.M. (MODIS/Aqua daytime overpass time) and 1:30 A.M. (MODIS/Aqua nighttime overpass time), (3) differences between 10:30 A.M. (MODIS/Terra daytime overpass time) and 10:30 P.M. (MODIS/Terra nighttime overpass time), (4) differences between 10:30 A.M. and 1:30 A.M., and (5) differences between 1:30 P.M. and 10:30 P.M. *A*, *B*, and *C* are the constant coefficients corresponding to different input schemes, which are obtained from model-simulated data under different atmospheres and surface characteristic conditions. From an atmosphere–land exchange (ALEX) model simulation analysis, Equation (7) with differences between 1:30 P.M. and 1:30 A.M. as inputs, *i.e.*, ΔT_s, ΔT_a, and ΔR_n equal the values of T_s, T_a, and R_n at 1:30 P.M. minus that at 1:30 A.M., can better estimate daily EF than other input schemes, and coefficients A, B, and C corresponding to the input scheme are −14.74, 40.01, and 14.57 W/(m^2·K), respectively. More details on the theoretical background and derivation of equation (7) are found in the paper of Lu *et al.* (2013) [38].

Incoming solar radiation (R_g) is the main driving source of surface energy [43]. Figure 1 shows the relationships between R_n and R_g based on ALEX-simulated data and *in situ* measurements. It can be inferred that R_n is generally positively proportional to R_g with a coefficient of determination (R^2) larger than 0.98. Therefore, ΔR_n in Equation (7) can be further replaced by ΔR_g but with different coefficients.

Figure 1. Relationships between surface net radiation (R_n) and incoming solar radiation (R_g) based on ALEX-simulated data with different surface characteristics for three representative clear days and *in situ* measurements at the US-SRC station for clear skies in 2011 (see Section 3). Atmosphere forcing driven the ALEX model was measured at the Yucheng station on 24 April, 29 May, and 21 July 2010, and more details can be found in the Appendix of [38].

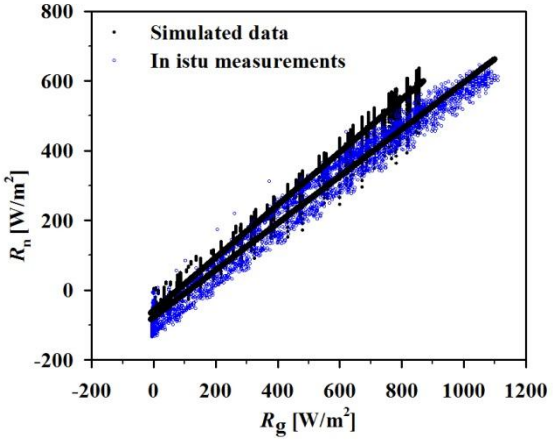

Using ΔR_g as an input variable of Equation (7) can obviate the calculation for longwave radiation. Furthermore, estimating R_g from remotely sensed data is easier than estimating R_n. Another purpose for using ΔR_g is that there is no incoming solar radiation at night, and only a one-time measurement of R_g in a day can meet the input requirements of Equation (7). Constant coefficients A, B, and C in Equation (7) corresponding to the input variable ΔR_g are obtained using the ALEX-simulated data under different surface and atmospheric conditions. Daily EF is consequently expressed as follows:

$$EF_{\text{daily}} = 1 - (-13.52 \times f_c^{\,2} + 41.81 \times f_c + 24.26)\frac{\Delta T_s - \Delta T_a}{\Delta R_g} \quad (8)$$

where ΔT_s, ΔT_a, and ΔR_g are the differences of T_s, T_a, and R_g between 1:30 P.M. and 1:30 A.M, respectively. With known f_c, ΔT_s, ΔT_a, and ΔR_g, daily EF can be calculated by Equation (8). When daily EF estimates with simulated data as inputs are compared with ALEX-simulated values, R^2 is 0.716 and a root mean square error (RMSE) is 0.129 (see Figure 2a). This result is similar to the estimation with ΔR_n as an input, which obtained an R^2 of 0.719 and an RMSE of 0.130 [38]. As shown in Figure 2b, daily EF estimates from two input schemes are nearly the same. Therefore, the substitute for ΔR_n with ΔR_g seems to be reasonable for daily EF estimates.

Figure 2. Comparisons of daily evaporative fraction (EF) estimates from Equation (8) with (**a**) ALEX-simulated values and (**b**) the results using ΔR_n.

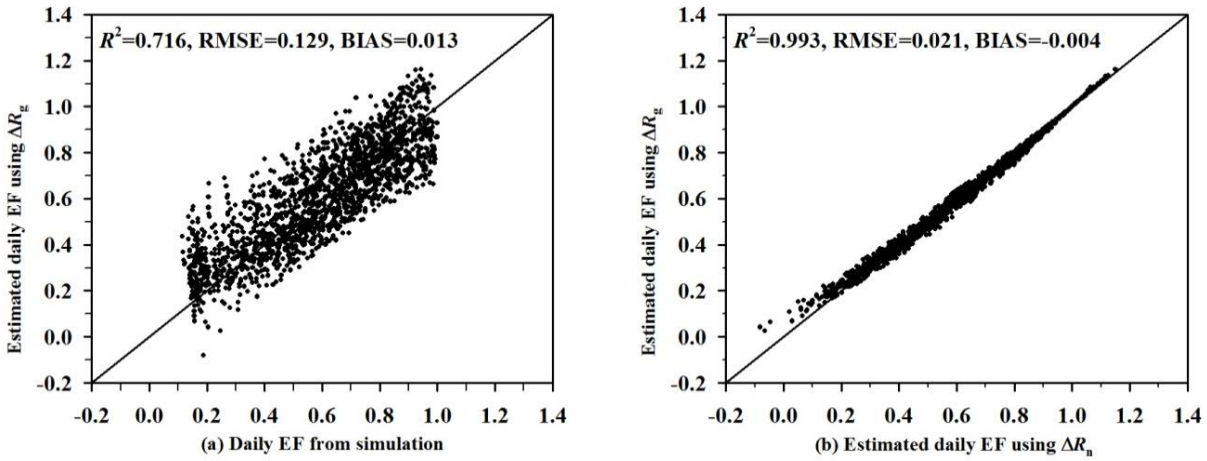

3. Data and Processing

3.1. Study Sites

The input variables of Equation (8) can be obtained from remotely sensed data. Because there are numerous uncertainties in the processes of retrieving surface parameters/variables [44,45], the ground-based measurements from six Ameriflux sites with different land covers are used to validate the performance of the EF parameterization scheme of Equation (8). Among these stations, five stations (US-Ne2, US-Seg, US-SRC, US-Me6, and US-UMB) are located in the United States, and one (BR-Sa3) is located in Brazil. Land use and land cover at the stations include croplands (CRO), grasslands (GRA), open shrublands (OSH), evergreen needleleaf forests (ENF), deciduous broadleaf forests (DBF), and evergreen broadleaf forests (EBF), respectively (see Figure 3). The surface elevation varies from 234 to 1622 m, and the soil textures include deep silty clay loams, loamy sand, sandy loam, sandy lake deposits, and yellow dystrophic latosol. Basic information about these stations is listed in Table 1.

Figure 3. Distribution of sites for validation of EF parameterization scheme (The background is the land use type of 2012 classified according to the University of Maryland scheme, which is extracted from the Land Cover Type Climate Modeling Grid product MCD12C1 with 0.05 degree spatial resolution.).

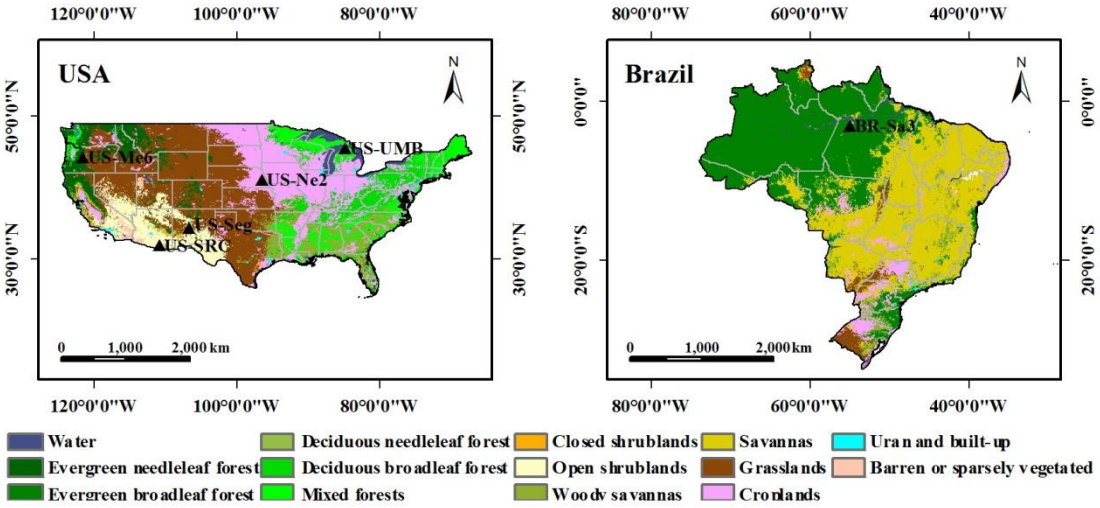

Table 1. Basic information for the six Ameriflux stations (CRO: croplands; GRA: grasslands; OSH: open shrublands; ENF: evergreen needleleaf forest; DBF: deciduous broadleaf forest; EBF: evergreen broadleaf forest).

Site ID	Site Name	Latitude	Longitude	Elevation (m)	Land Cover	Climate	Soil Texture
US-Ne2	Mead Irrigated Rotation	41.1649 °N	96.4701 °W	362	CRO	Temperate	Deep silty clay loams
US-Seg	Sevilleta Desert Grassland	34.3623 °N	106.7019 °W	1622	GRA	Semi-arid	Loamy sand
US-SRC	Santa Rita Creosote	31.9083 °N	110.8395 °W	991	OSH	Subtropical	Sandy loam
US-Me6	Metolius Young Pine Burn	44.3232 °N	121.6043 °W	996	ENF	Warm dry summers and cool wet winters	Sandy loam
US-UMB	UMBS	45.5598 °N	84.7138 °W	234	DBF	Temperate northern	Sandy lake deposits
BR-Sa3	LBA Tapajos KM83 Logged Forest	3.018 °S	54.971 °W	100	EBF	Tropical	Yellow dystrophic latosol

3.2. In situ Measurements

In situ measurements (meteorological variables, radiation data, and fluxes data from the eddy covariance (EC)) are collected from the Ameriflux network website [46] for the US-Ne2 station in 2011, the US-Seg station in 2010, the US-SRC station in 2011, the US-Me6 station in 2012, the US-UMB station in 2012, and the BR-Sa3 station in 2003. Collected T_a and R_g are directly used to drive the EF parameterization scheme of Equation (8). R_n, H, LE, and G are used to calculate the EC-measured daily EF and then to evaluate the EF estimates. The daily EF is calculated as the ratio of daily averaged LE to daily averaged R_n, neglecting the effect of G on EF at the daily scale. T_s is not directly measured at these sites. Incoming and outgoing longwave radiation (L_d and L_u) was used to calculate T_s by the equation of $T_s = ((L_u - (1-\varepsilon)L_d)/\sigma\varepsilon)^{1/4}$ with an assumption of 0.98 of surface emissivity (ε) in this study (σ is the Stefan–Boltzmann constant).

Averaged values of the main meteorological variables of precipitation, air temperature, and relative humidity in one year were calculated based on the collected data (see Table 2). Annual precipitation at six sites varied from 182 to 1461 mm, annual mean air temperature ranged from 8 to 25 ℃, and annual mean relative humidity ranged from 33% to 79%. There were missing measurements because of sensor malfunction, power outages, unfavorable weather, and other unknown reasons. Gaps in the missing data at the US-Ne2, US-Seg, and US-Me6 stations were filled by adopting the approach that combines measurement, interpolation, and empirical data synthesis [47], whereas the missing flux data at the US-SRC, US-UMB, and BR-Sa3 stations were not filled. Days with missing flux data were not considered in this study. Data at the US-Seg, US-SRC, US-Me6, and BR-Sa3 stations were averaged at a 30-min interval, whereas data at the Us-Ne2 and US-UMB stations were within 1 h.

Table 2. Summary of *in situ* measurements at six stations ($\overline{T_a}$ is the annual mean air temperature, ℃; $\overline{\mathrm{RH}}$ is the annual mean relative humidity, %.)

Site ID	Year	Precipitation (mm)	$\overline{T_a}$ (℃)	$\overline{\mathrm{RH}}$ (%)	Filled	Temporal Resolution
US-Ne2	2011	805	10	75	Yes	Hourly
US-Seg	2010	182	14	41	Yes	Half-hourly
US-SRC	2011	229	20	33	No	Half-hourly
US-Me6	2012	596	8	65	Yes	Half-hourly
US-UMB	2012	603	9	71	No	Hourly
BR-Sa3	2003	1461	25	79	No	Half-hourly

The EF parameterization scheme in Section 2 was derived under the assumption that EF was relatively invariant during the daytime, which most frequently occurs on cloud-free days with high radiation and humidity [41]. An automatic procedure based on Tang *et al.* (2013) [48] was developed to select available data for days in which EF was relatively invariant. Automated techniques were designed considering that (1) the maximum of R_g in a day occurs in the midday between 11:00 and 13:00; (2) R_g increases monotonically from sunrise to midday and decreases monotonically from midday to sunset; (3) days with daily (24 h) averaged R_g < 100 W/m^2 because of low solar radiation, which may occur in winter or be caused by full cloud cover during a day, are excluded; (4) days with daily mean T_a < 0 due to low solar radiation and with ΔT_s and ΔT_a less than 0 that were probably influenced by nighttime cloud are excluded. Days having a measured daily EF < 0 and > 1 were also

not utilized. A total of 408 cloud-free days were selected at these stations including 95 days in 2011 at the US-Ne2 station, 71 days in 2010 at the US-Seg station, 118 days in 2011 at the US-SRC station, 79 days in 2012 at the US-Me6 station, and 45 days in 2012 at the US-UMB station (see filled circles in Figure 4). Cloud-free days were not observed at the BR-Sa3 station in 2003 because of strong convective weather in the tropical region.

Figure 4. Distribution of clear days and partly clear days in one year.

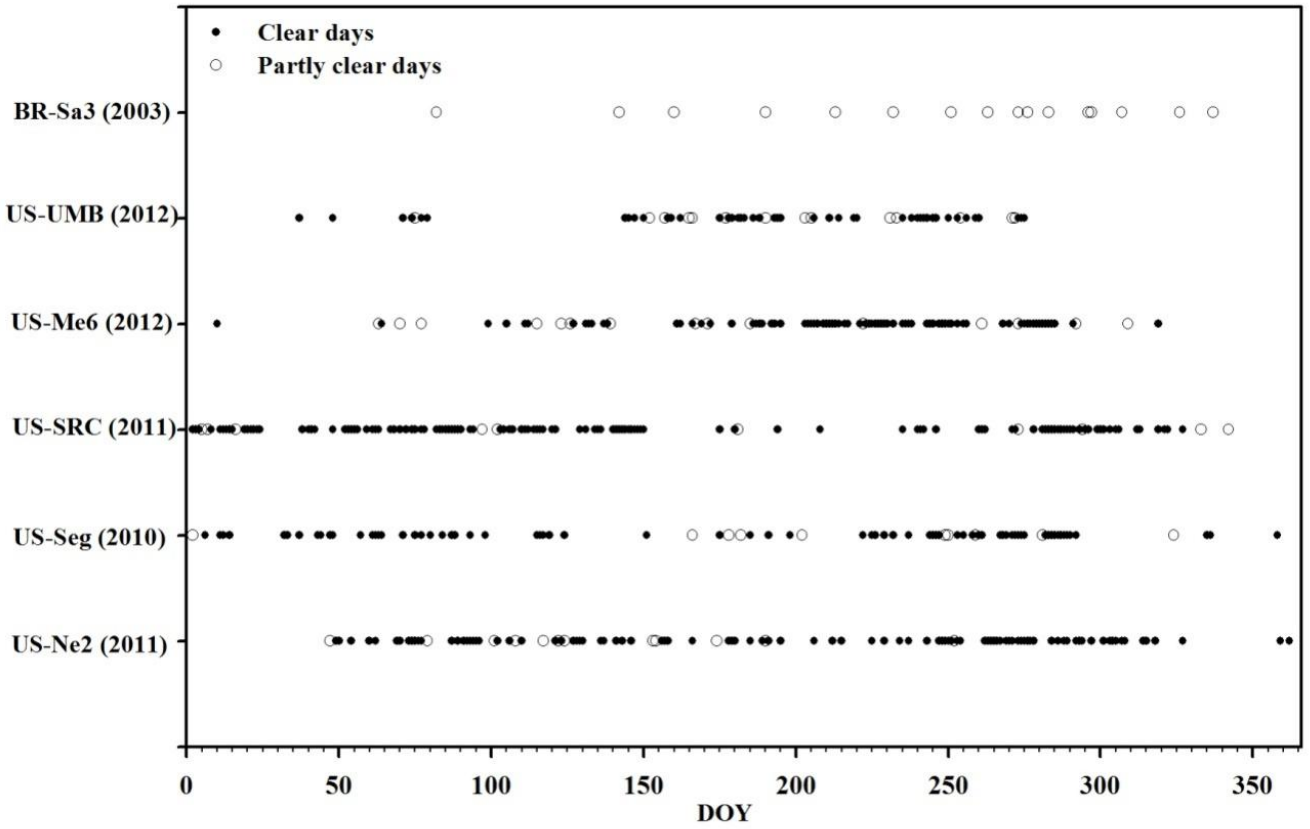

Because remote sensing observations represent a snapshot in time, it is not easy to judge whether an entire day is clear using remotely sensed data. Therefore, the performance of EF parameterization for partly clear days, *i.e.*, no cloud cover during the afternoon here, will also be discussed in this study. For the selection of partly clear days, the automatic procedure for judging clear days is equally applicable but not to regard the monotonic increase from sunrise to midday. A total of 77 partly clear days (marked by open circles in Figure 4) were selected including 12, 10, 10, 15, 14, 16 partly clear days at the US-Ne2 station, at the US-Seg station, at the US-SRC station, at the US-Me6 station, at the US-UMB station, and at the BR-Sa3 station, respectively.

The energy balance non-closure in EC-based measurements was frequently reported in many previous studies [49]. As shown in Figure 5, daily average $H + LE$ are all less than daily average $R_n - G$ for clear and partly clear skies at the six sites. The mean energy balance ratio (EBR) is ~0.83, and the RMSE is ~25 W/m^2. For each site, the daily-scale statistics of energy balance closure of EC-based measurements including EBR, R^2, RMSE, and BIAS are listed in Table 3. The most serious energy balance non-closure in EC-based measurements occurs at the US-Me6 station with a mean

EBR of 0.78, and the RMSE between $H + LE$ and $R_n - G$ is 35.2 W/m^2. At the BR-Sa3 station, the EC-measured daily average $H + LE$ is closer to $R_n - G$ with an EBR of 0.93. In general, the inconsistent source areas between radiation flux ($R_n - G$) and turbulent flux ($H + LE$), and neglecting some terms in surface energy balance equation such as storage heat in forest vegetation, the energy due to photosynthesis and advection, may be the main reasons for non-closure in the energy balance from EC-based measurements.

Figure 5. Comparisons of daily average $H + LE$ from EC-based measurements with daily average $R_n - G$ for clear and partly clear skies at six Ameriflux sites.

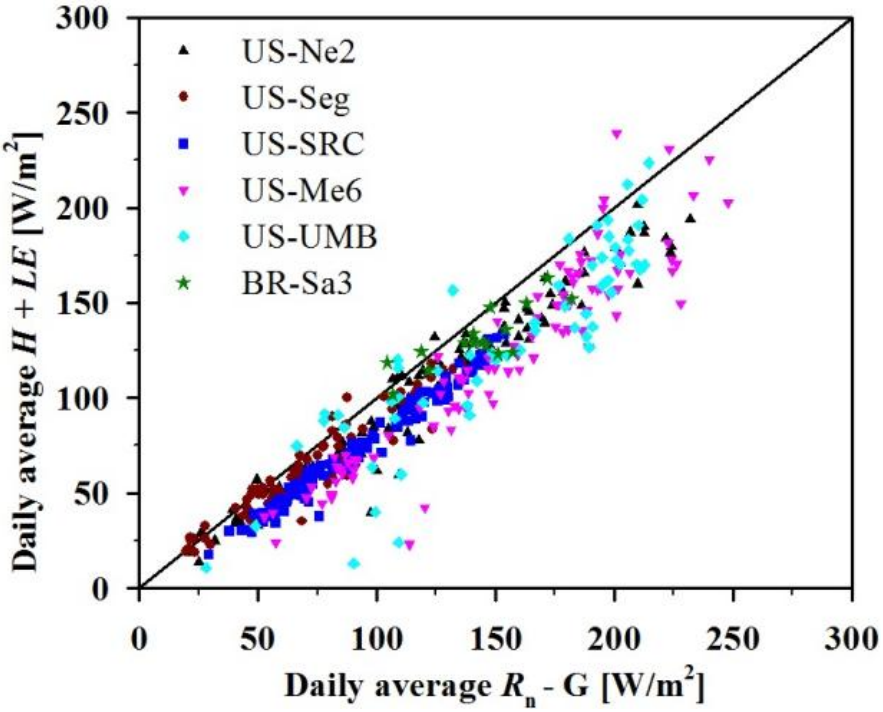

Table 3. Statistics of energy balance closure of EC-based measurements at the daily scale (EBR is the energy balance ratio, which is the mean value of the ratio of daily average $H+LE$ to daily average $R_n - G$)

Site ID	Year	EBR	R^2	RMSE (W/m^2)	BIAS (W/m^2)
US-Ne2	2011	0.86	0.951	20.7	−16.6
US-Seg	2010	0.90	0.906	12.9	−8.6
US-SRC	2011	0.79	0.975	20.1	−19.3
US-Me6	2012	0.78	0.872	35.2	−30.1
US-UMB	2012	0.84	0.791	33.1	−23.5
BR-Sa3	2003	0.93	0.678	16.7	−11.5

3.3. Fractional Vegetation Cover f_c

Apart from the variables ΔT_s, ΔT_a, and ΔR_g, f_c is also required as an input for the EF parameterization scheme presented as Equation (8). Because of the lack of *in situ* measurements for vegetation cover, MOD13Q1 and MYD13Q1 products in the spatial resolution of 250 m, which

provide the normalized difference vegetation index (NDVI) every 16 days, are combined to calculate f_c every 8 days by linear mixture modeling [50], and computed using Equation (9):

$$f_c = \frac{\text{NDVI-NDVI}_{\min}}{\text{NDVI}_{\max}\text{-NDVI}_{\min}} \quad (9)$$

where $\text{NDVI}_{\min}$ and $\text{NDVI}_{\max}$ are the NDVI for bare soil and dense vegetation at full coverage, respectively. $\text{NDVI}_{\min}$ and $\text{NDVI}_{\max}$ are not only determined by surface characteristics but also are dependent on remotely sensed image data. For bare soil, NDVI tends to vary between −0.1 and 0.2 [13], but in this study, $\text{NDVI}_{\min}$ is given as 0. For dense vegetation, NDVI depends on vegetation type, age, and leaf water content. Carlson *et al.* (1990) [51] mentioned that the upper limit of NDVI for dense vegetation is in the range of 0.5–0.8, whereas Prihodko and Goward (1997) [52] used the observation of reflectance and transmittance in the red and near-infrared wavelengths from the FIFE information system to compute the NDVI of an infinitely thick canopy for each species, and obtained an average NDVI of 0.86 for the full canopy. Determination of the value of $\text{NDVI}_{\max}$ for different surface characteristics is not easy. $\text{NDVI}_{\max}$ is set as 0.86 for all sites here. Because the scattering coefficients for the leaves and the soil, the leaf-area index, the leaf angle distribution, and the angle of incident radiation affect the NDVI, the vegetation cover problem becomes more complex [13]. The errors in EF estimation caused by the uncertainty of f_c will be discussed in Section 4.2.

4. Results and Discussions

4.1. Daily EF Estimates for Clear Skies and Partly Clear Skies

For 408 cloud-free days, with known ΔT_s, ΔT_a, and ΔR_g from *in situ* measurements and f_c from remotely sensed data, daily EF was estimated using Equation (8). Compared with EC-based measurements, daily EF was overestimated by 0.212 (see black triangles in Figure 6a). The overestimation was mainly caused by the underestimation of *LE* from EC measurements. Two methods were frequently used to correct EC-measured *LE*, *i.e.*, the residual energy (RE) method and the Bowen ratio (BR) method [49]. The *LE* corrected by the RE method is equal to $R_n - G - H$ with the assumption of relatively accurate measurements for *H*. The BR method is to assume that the non-closure of energy balance is not only caused by EC-measured *LE* but also by EC-measured *H*. The imbalance of energy is partitioned into *H* and *LE* according to the Bowen ratio, *i.e.*, $H_{\_BR} = H \times (R_n - G) / (H + LE)$ and $LE_{\_BR} = LE \times (R_n - G)/(H + LE)$. The corrected *LE* is then used to calculate EC-measured daily EF. When the estimated EF from Equation (8) is compared with the BR/RE-corrected EF, the overestimation in EF is reduced (see green circles and blue symbols in Figure 6a, respectively). Daily EF estimates are closer to the RE-corrected EF, showing an RMSE of 0.152 and an R^2 of 0.586. For selected 77 partly clear days, daily EF estimates from Equation (8) are also closer to the RE-corrected daily EF with an R^2 of 0.549 and an RMSE of 0.171 (see Figure 6b). The result indicates that the EF parameterization scheme of Equation (8) can also be applied to estimate daily EF for partly clear skies, which mainly occur during the afternoon.

Figure 6. Comparisons of daily EF estimates with values from EC measurements, the Bowen ratio (BR) correction method, and the residual energy (RE) correction method for **(a)** clear skies and **(b)** partly clear skies.

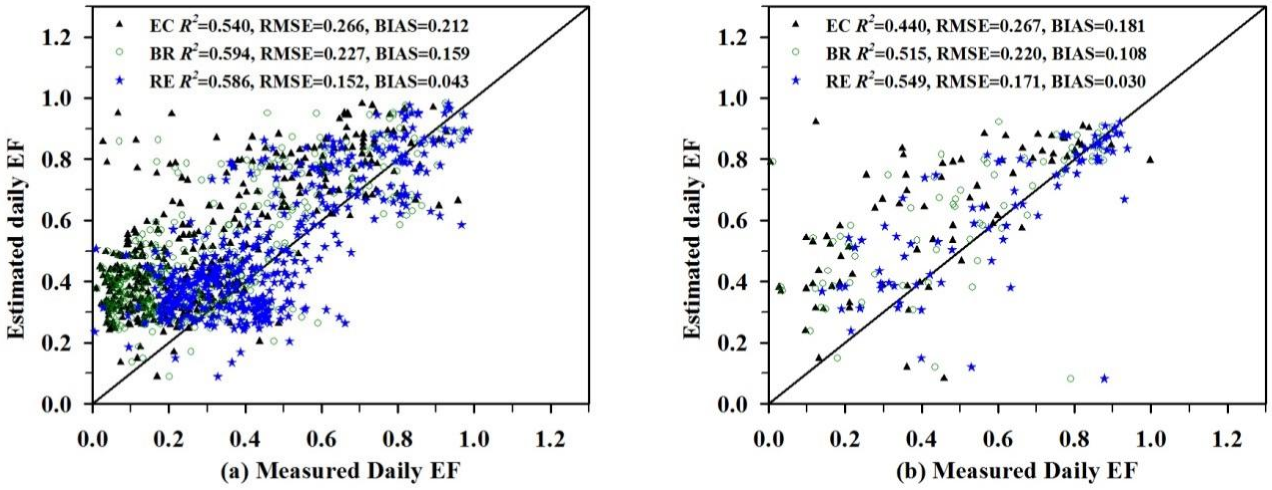

4.2. Uncertainty in EF Estimates Caused by f_c

Uncertainty in determining input variable f_c is also a source of error for daily EF estimates. Because f_c is from the 16-day MODIS NDVI products at spatial resolution of 250 m, the different temporal and spatial scales between *in situ* measurements and the MODIS sensor could result in discrepancies between estimated daily EF and measured values. Sensitivity and error analysis for f_c made by [38] concluded that 0.2 variations in f_c can lead to approximately 0.1 mean variations in daily EF estimates. Different schemes for calculating f_c and the assignments for $NDVI_{max}$ and $NDVI_{min}$ can produce different daily EF estimates (see Figure 7 and Table 4). f_c from a non-linear model relating to NDVI [53], *i.e.*, the square of equation (6), is less than that from the linear model with an RMSE of 0.183 (see filled triangles in Figure 7a). The underestimation in f_c will cause the overestimation of daily EF according to the mathematical formulation of equation (8). Therefore, when f_c from the non-linear model is used as an input for equation (8), daily EF estimates are greater than the results from the linear model with an RMSE of ~0.1 (see filled triangles in Figure 7b). The larger bias is on the lower range of EF values, most of which are related to the condition of low f_c. When the $NDVI_{max}$ and $NDVI_{min}$ in the linear model of Equation (6) are given as 0.66 and 0.2, respectively [51,53], f_c is less than the values calculated by 0 and 0.86 as inputs for low f_c. The opposite is true for high f_c (see open circles in Figure 7a). For daily EF estimates, the RMSE caused by different assignments for $NDVI_{max}$ and $NDVI_{min}$ is also ~0.1 (see open circles in Figure 7b). Those open circles deviating from the 1:1 line in Figure 7b correspond to low f_c conditions, which are attributed to underestimation of f_c. The larger bias also occurs at the lower EF condition. Therefore, daily EF estimation from Equation (8) is more sensitive to low f_c, particularly for a low ET surface. The implicit assumption in Equation (8) that EF is relatively invariant during the daytime may be valid at this situation. Sensitivity of EF estimates to low ET surfaces is similar to the findings of Long *et al.* (2014) [54], where uncertainties among the ET products increased with aridity. A low ET surface is generally related to

low soil water content. Further study is required to determine if soil water content can be used as an input parameter for Equation (8), and to find the best approach for parameterizing the EF equation.

Figure 7. Comparisons of (**a**) f_c from different schemes and (**b**) daily EF estimates corresponding to different f_c ($f_{c\_non\text{-}linear}$ represents the results from a non-linear model; $f_{c\_0.2/0.66}$ denotes the results for $NDVI_{min}$ = 0.2 and $NDVI_{max}$ = 0.66).

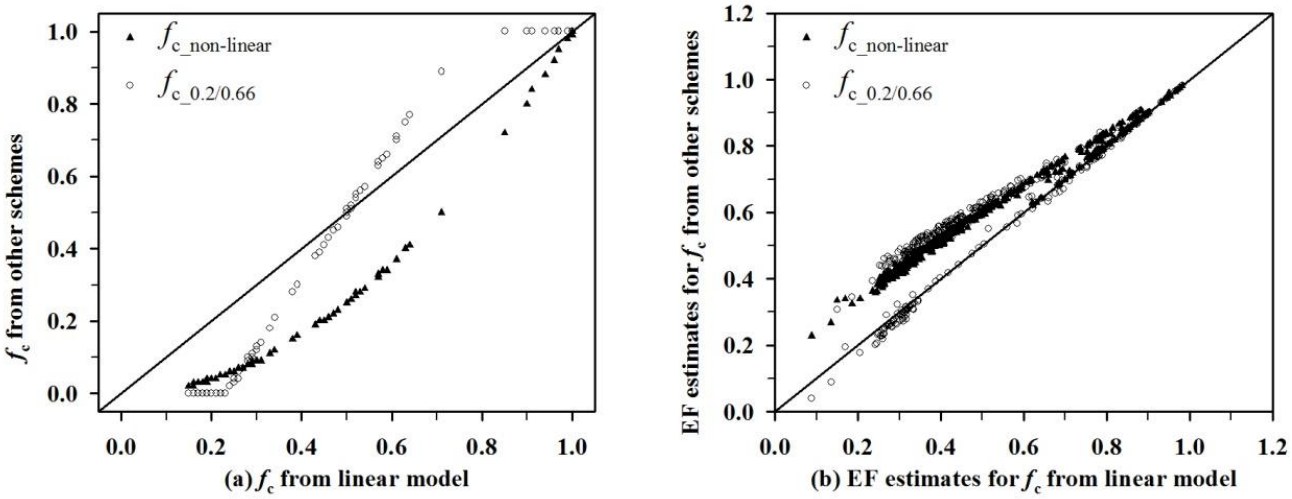

Table 4. Results of f_c from different schemes and corresponding daily EF estimates compared with those values from the linear model ($f_{c\_non\text{-}linear}$ represents the results from a non-linear model; $f_{c\_0.2/0.66}$ denotes the results for $NDVI_{min}$ = 0.2 and $NDVI_{max}$ = 0.66).

	$f_{c\_non\text{-}linear}$	$EF\_{non\text{-}linear}$	$f_{c\_0.2/0.66}$	$EF\_{0.2/0.66}$
R^2	0.964	0.990	0.966	0.879
RMSE	0.183	0.100	0.155	0.101
BIAS	-0.167	0.088	−0.099	0.070

4.3. Performance of EF Parameterization Scheme for Different Land Covers

The six stations used in this study correspond to six different land covers. Daily EF estimates for clear days and partly clear days were both considered in this section. The estimated EF for each station is compared with the RE-corrected EF, which is shown in Figure 8. Most of the absolute biases of daily EF estimates from Equation (8) for different vegetation types are less than 0.1, and the RMSEs are not more than 0.2. The estimated daily EF for CRO and OSH surfaces are correlated more strongly to the RE-corrected EF with the R^2 of 0.640 and 0.650, respectively. For those surfaces covered by GRA, ENF, DBF, and EBF vegetation types, most results appear to be consistent with the RE-corrected EF, but some scatter points and relatively concentrated distribution of daily EF lead to the low R^2. It seems that surface elevation and soil texture have no obvious contribution to the errors of EF estimates, *i.e.*, the errors of EF estimates do not strongly depend on surface elevation and soil texture. Errors of daily EF estimates, daily averaged R_g, daily total precipitation, f_c, and $\Delta T_s - \Delta T_a$ of six stations are displayed in Figures 9–14 to further evaluate the reason for discrepancies.

Figure 8. Comparisons of daily EF estimates with the EF corrected by the residual energy (RE) method for different underlying surfaces, (**a**) croplands (CRO), (**b**) grasslands (GRA), (**c**) open shrublands (OSH), (**d**) evergreen needleleaf forest (ENF), (**e**) deciduous broadleaf forest (DBF), and (**f**) evergreen broadleaf forest (EBF).

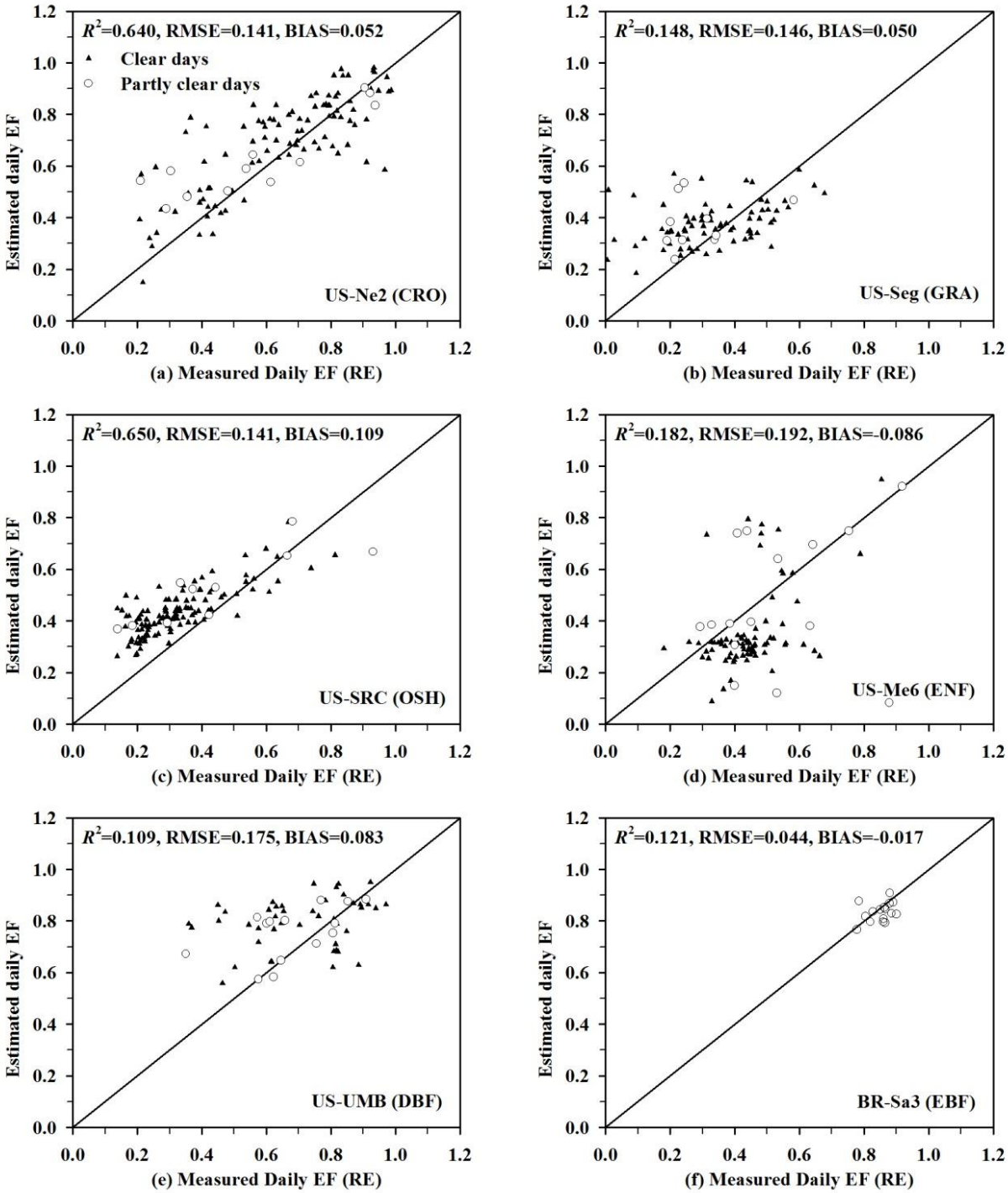

(1) For the surface covered by CRO vegetation types, which is at the US-Ne2 station, a majority of the EF estimates are satisfied (see Figure 8a), and the errors vary from −0.2 to 0.2 (see Figure 9). Several large errors (>0.3) for EF estimates occur on DOY 75, 79, 128, 129, 293, 294, 359, and 362 (marked by red circles in Figure 9). The overestimation on DOY 75 may be mainly caused by the

small value of $\Delta T_s - \Delta T_a$, which is mostly from measurement errors or is influenced by high wind speed (wind speed in the afternoon at approximately 13:30 on DOY 75 is ~9 m/s). The error on DOY 79 could be attributed to the effect of clouds, and obvious low averaged R_g was observed on the day. The overestimation on DOY 128, 129, 293, and 294 may be due to the underestimation in f_c. On DOY 359 and 362, low R_g that occurred in winter may be the main reason leading to the negative biases of EF estimates. This is because under the condition of low solar radiation, the implicit assumption of relatively invariant EF in Equation (8) is not well met. In general, under the condition of strong solar radiation, sufficient soil water content, dense vegetation cover, and low $\Delta T_s - \Delta T_a$, errors in EF estimates are relatively small.

Figure 9. Error in EF estimates, daily averaged incoming solar radiation (R_g), fractional vegetation cover (f_c), and $\Delta T_s - \Delta T_a$ at the US-Ne2 station for all selected clear days and partly clear days, and daily precipitation (P) for all days in one year.

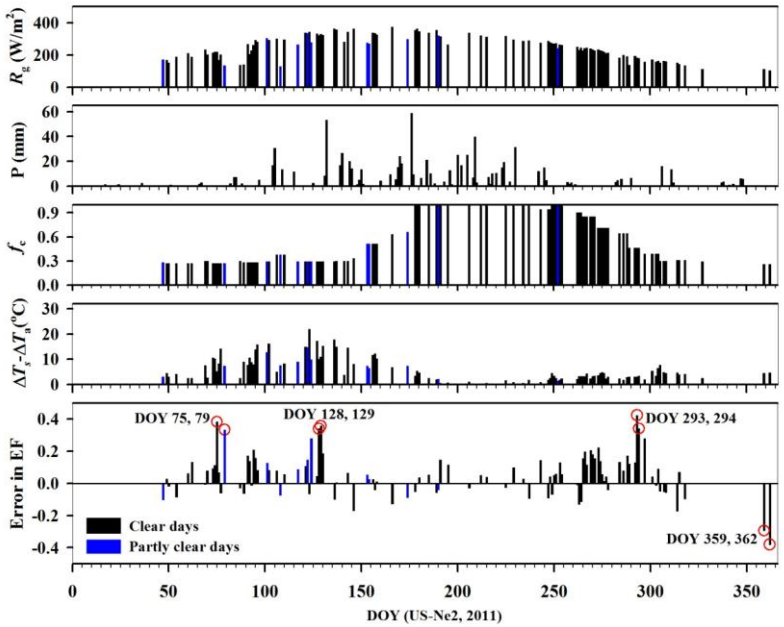

(2) At the US-Seg station covered by GRA vegetation type, the climate is semi-arid, and the annual precipitation of the region is ~230 mm, with a major portion (>50%) occurring in a summer rainy season, July to September [55]. In 2010, the total precipitation was only 182 mm (see Table 2). Therefore, EF from measurements at the US-Seg station was generally low, even less than 0.6 (see Figure 8b). Most of the EF estimates from Equation (8) generally fall into this range but with a slight overestimation. According to Equation (8), the underestimation in f_c would lead to an overestimation in EF. Therefore, low f_c of ~0.2 in 2010 (may be underestimated) results in the overestimation of EF at the US-Seg station. On DOY 6, 336, and 358, larger errors may be caused by low solar radiation in winter (see Figure 10). The relatively concentrated distribution of daily EF at the US-Seg station in 2010, approximately from 0.2 to 0.6, may lead to the low R^2 of 0.148 in Figure 8b.

Figure 10. Error in EF estimates, daily averaged incoming solar radiation (R_g), fractional vegetation cover (f_c), and $\Delta T_s - \Delta T_a$ at the US-Seg station for all selected clear days and partly clear days, and daily precipitation (P) for all days in one year.

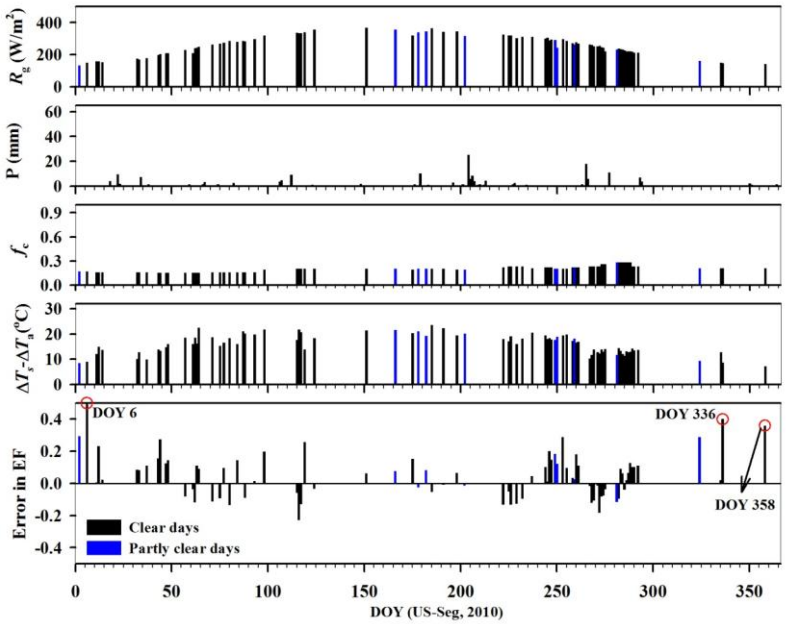

(3) At the US-SRC station, most of daily EF values lie in the range of 0.1 to 0.6 (see Figure 8c). This may be related to low precipitation of ~229 mm and low vegetation cover of ~0.3 in 2011 (see Table 2 and Figure 11, respectively). Although the R^2 between the estimated EF and measured values is high, there is an overestimation when measured EF is low (See Figure 8c). As analyzed in Section 4.2, Equation (8) is more sensitive to low f_c for daily EF estimates, particularly for a low ET surface. It is difficult to accurately determine f_c particularly at the sparse vegetation surface covered by OSH types. Therefore, the potential underestimation in f_c may lead to the overestimation of daily EF at the US-SRC station. The obvious underestimation on DOY 5 was primarily because of the effect of clouds. The positive biases on DOY 93 and DOY 149 were from the relative low values of $\Delta T_s - \Delta T_a$ probably due to high wind speed (wind speeds at approximately 13:30 on DOY 93 and DOY 149 were ~6 m/s and 8 m/s, respectively). The energy balance non-closure in EC-based measurements at this station with the EBR of 0.79 (see Table 3) may have led to discrepancies between the estimated EF and measured values.

(4) At the US-Me6 station covered by evergreen needleleaf forest, the simplified EF parameterization scheme gave the worst results with an RMSE of 0.192 (see Figure 8d), and most of the EF was underestimated (see Figure 12). This may be related to the local climate having warm dry summers and cool wet winters. Most precipitation (~97% of annual rainfall) falls between October and June. The climatic condition of the warm dry summer and cool wet winter may not easily meet the assumption of Equation (8) because EF during the daytime is relatively invariant when there is high radiation and humidity. The underestimation of EF on DOY 70 and 123 and the overestimation on DOY 139 and 171 may result from clouds, whereas the overestimation on DOY 138 and 161 was evidently from low values of $\Delta T_s - \Delta T_a$ due to high wind speed of ~6 m/s. There was no precipitation on DOY 189, 192, 193, and 195, *i.e.*, there was insufficient water in the soil, resulting in less ET on

these days. The low EF from Equation (8) seems more reasonable; therefore, large negative biases on DOY 189, 192, 193, and 195 were attributed to the uncertainty in measurements or the errors from the RE correction method. As shown in Table 3, energy balance non-closure is most noticeable for EC-based measurements that occurred at this station.

Figure 11. Error in EF estimates, daily averaged incoming solar radiation (R_g), fractional vegetation cover (f_c), and $\Delta T_s - \Delta T_a$ at the US-SRC station for all selected clear days and partly clear days, and daily precipitation (P) for all days in one year.

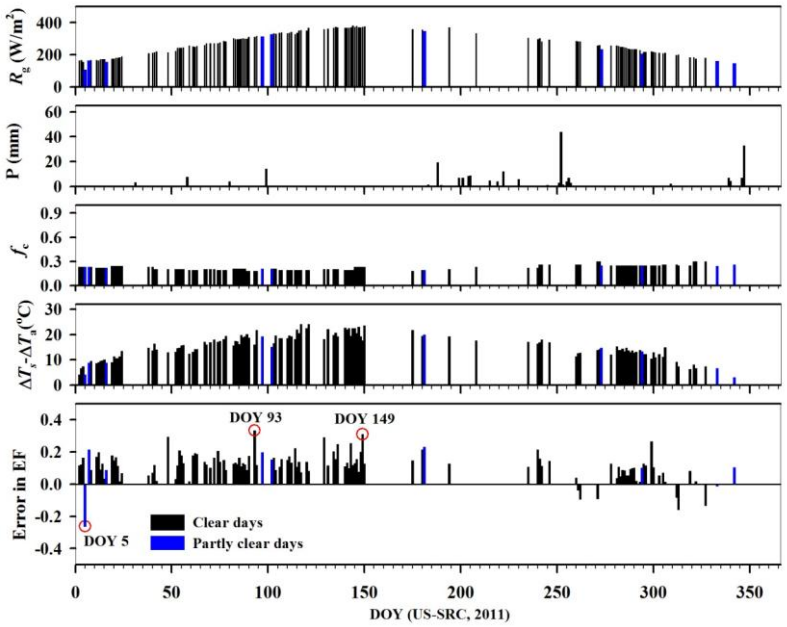

Figure 12. Error in EF estimates, daily averaged incoming solar radiation (R_g), fractional vegetation cover (f_c), and $\Delta T_s - \Delta T_a$ at the US-Me6 station for all selected clear days and partly clear days, and daily precipitation (P) for all days in one year.

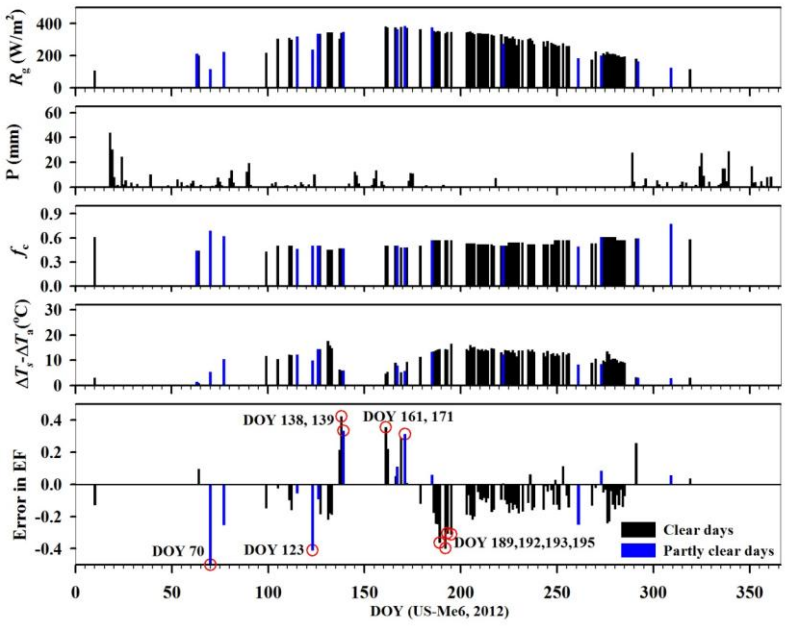

Figure 13. Error in EF estimates, daily averaged incoming solar radiation (R_g), fractional vegetation cover (f_c), and $\Delta T_s - \Delta T_a$ at the US-UMB station for all selected clear days and partly clear days, and daily precipitation (P) for all days in one year

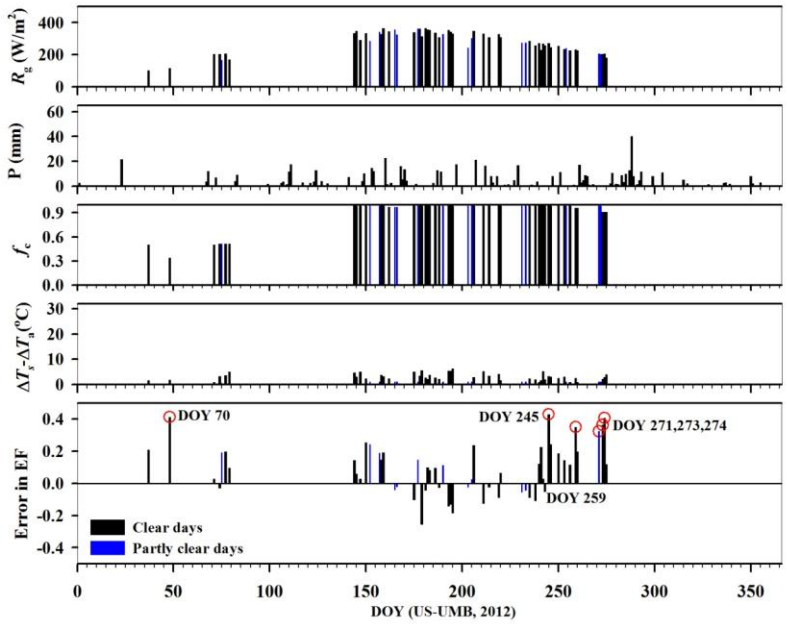

Figure 14. Error of EF estimates, daily averaged incoming solar radiation (R_g), fractional vegetation cover (f_c), and $\Delta T_s - \Delta T_a$ at the BR-Sa3 station for all selected clear days and partly clear days, and daily precipitation (P) for all days in one year

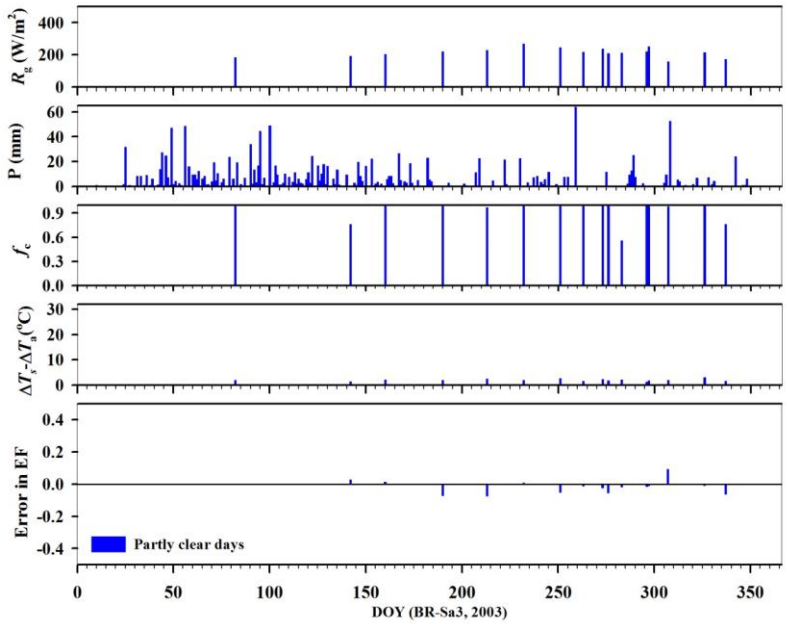

(5) For the surface covered with deciduous broadleaf forest, daily EF mainly varies from 0.5 to 1 (see Figure 8e). This is related to the temperature and humidity climate at the US-UMB station with a mean temperature of 9 ℃ and total precipitation of 609 mm in 2012 (see Table 2). The overestimation on DOY 70 may be caused by low solar radiation and underestimation in f_c (see Figure 13). During the

summer days from June to September, the surface is completely covered by broadleaf vegetation, and soil moisture is ample. Under this condition, high ET value is more reasonable. Therefore, the large overestimation of EF on DOY 245, 259, 271, 273, and 274 may be from the uncertainty in measurements or errors for energy imbalance correction.

(6) The rainy tropical climate results in high EF of ~0.8 at the BR-Sa3 station covered by evergreen broadleaf forest (EBF) during one year (see Figure 8f), being coincident with the estimated values close to 0.8. The concentrated distribution of EF during one year leads to low R^2. Although the data displayed in Figure 14 occurred on partly clear days, there is not an obvious large bias for daily EF estimates at this station. The abundant rainfall and dense vegetation led to the low values of $\Delta T_s - \Delta T_a$ and reduced the effects of clouds on EF estimates.

5. Conclusions

Lu *et al.* (2013) [38] developed a method for estimating daily evaporative fraction (EF) derived by day–night differences in surface temperature (T_s), air temperature (T_a), and net radiation (R_n). Because incoming solar radiation (R_g) can be readily estimated from remotely sensed data and there is a strong relationship between R_g and R_n, this study simplified the equation for estimating daily EF using R_g. The accuracy of the simplified EF parameterization scheme with ΔR_g as an input is nearly equivalent to that with ΔR_n as an input.

When *in situ* measurements from Ameriflux sites are used to drive the simplified parameterization scheme, daily EF estimates for clear days are closer to the RE-corrected daily EF with a coefficient of determination of 0.586 and a root mean square error of 0.152. It is not an easy thing to judge the sky condition using several remote sensing observations. However, the developed method can be used to estimate daily EF for partly clear days with the accuracy similar to that for clear sky condition. Errors from the correction for energy imbalance in EC-based measurements and the uncertainty in calculating fractional vegetation cover (f_c) are the primary factors that lead to discrepancies between estimated and measured daily EF. Daily EF estimates from the simplified parameterization scheme are more sensitive to low f_c conditions with low ET surfaces. Analyses of daily EF estimates at six vegetation surfaces indicate that the constant coefficients in the simplified EF parameterization scheme are not strongly site-specific, and could be applied to different land covers with reasonable accuracy if surface vegetation cover can be accurately determined. EF estimates are more accurate for regions that are characteristically warm and humid with strong solar radiation and adequate soil water content.

The input requirements of relatively few variables that can be easily obtained from remotely sensed data, *i.e.*, the day–night difference in surface and air temperatures, can reduce uncertainties in EF estimates due to retrieval error from remote sensing. Only by using the parameters/variables of f_c, ΔT_s, ΔT_a, and ΔR_g, can Equation (8) estimate daily EF, which can be further used to partition the surface available energy into sensible and latent heat fluxes. Although the accuracy of the EF parameterization scheme is acceptable, there is still room for improving the model, particularly for low ET surfaces with low f_c. Further study should be directed toward improving daily EF estimates by introducing other retrieval variables from remote sensing, such as soil moisture.

Acknowledgments

We thank the AmeriFlux Principal Investigators who provided data for our project through the Ameriflux network website (http://ameriflux.ornl.gov/). We greatly thank Di Long from the Bureau of Economic Geology, Jackson School of Geosciences, The University of Texas at Austin, who provided many excellent suggestions for improving this study. This work was supported by the National Natural Science Foundation of China under Grant 41201366 and 41101332. The authors would like to thank Enago (www.enago.cn) for the English language review.

Author Contributions

Jing Lu mainly wrote the manuscript and was responsible for the research design, data preparation and analysis. Ronglin Tang, Huajun Tang, and Zhao-Liang Li assisted in methodology development and research design, and also participated in manuscript writing and revision. Yuyun Bi and Kun Shao participated in data collection and processing. Guoqing Zhou and Jelila Labed performed the data validation analysis, and helped polish the language of this manuscript.

Conflicts of Interest

The authors declare no conflict of interest.

References and Notes

1. Oki, T.; Kanae, S. Global hydrological cycles and world water resources. *Science* **2006**, *313*, 1068–1072.
2. Trenberth, K.E.; Fasullo, J.T.; Kiehl, J. Earth's global energy budget. *Bull. Amer. Meteor. Soc.* **2009**, *90*, 311–323.
3. Kalma, J.D.; McVicar, T.R.; McCabe, M.F. Estimating land surface evaporation: A review of methods using remotely sensed surface temperature data. *Surv. Geophys.* **2008**, *29*, 421–469.
4. Li, Z.-L.; Tang, R.L.; Wan, Z.M.; Bi, Y.Y.; Zhou, C.H.; Tang, B.H.; Yan, G.J.; Zhang, X.Y. A review of current methodologies for regional evapotranspiration estimation from remotely sensed data. *Sensors* **2009**, *9*, 3801–3853.
5. Su, Z. The Surface Energy Balance System (SEBS) for estimation of turbulent heat fluxes. *Hydrol. Earth Syst. Sci.* **2002**, *6*, 85–99.
6. Bastiaanssen, W.; Menenti, M.; Feddes, R.; Holtslag, A. A remote sensing surface energy balance algorithm for land (SEBAL). 1. Formulation. *J. Hydrol.* **1998**, *212*, 198–212.
7. Norman, J.M.; Kustas, W.P.; Humes, K.S. Source approach for estimating soil and vegetation energy fluxes in observations of directional radiometric surface-temperature. *Agric. For. Meteorol.* **1995**, *77*, 263–293.
8. Allen, R.G.; Tasumi, M.; Trezza, R. Satellite-based energy balance for mapping evapotranspiration with internalized calibration (METRIC)—Model. *J. Irrig. Drain. E. ASCE* **2007**, *133*, 380–394.
9. Mu, Q.Z.; Zhao, M.S.; Running, S.W. Improvements to a MODIS global terrestrial evapotranspiration algorithm. *Remote Sens. Environ.* **2011**, *115*, 1781–1800.

10. Long, D.; Singh, V.P. A two-source trapezoid model for evapotranspiration (TTME) from satellite imagery. *Remote Sens. Environ.* **2012**, *121*, 370–388.
11. Tang, R.L.; Li, Z.-L.; Jia, Y.Y.; Li, C.R.; Sun, X.M.; Kustas, W.P.; Anderson, M.C. An intercomparison of three remote sensing-based energy balance models using Large Aperture Scintillometer measurements over a wheat–corn production region. *Remote Sens. Environ.* **2011**, *115*, 3187–3202.
12. Li, Z.-L.; Wu, H.; Wang, N.; Qiu, S.; Sobrino, J.A.; Wan, Z.M.; Tang, B.H.; Yan, G.J. Land surface emissivity retrieval from satellite data. *Int. J. Remote Sens.* **2013**, *34*, 3084–3127.
13. Wittich, K.; Hansing, O. Area-averaged vegetative cover fraction estimated from satellite data. *Int. J. Biometeorol.* **1995**, *38*, 209–215.
14. Bisht, G.; Venturini, V.; Islam, S.; Jiang, L. Estimation of the net radiation using MODIS (Moderate Resolution Imaging Spectroradiometer) data for clear sky days. *Remote Sens. Environ.* **2005**, *97*, 52–67.
15. Tang, B.H.; Li, Z.-L.; Zhang, R.H. A direct method for estimating net surface shortwave radiation from MODIS data. *Remote Sens. Environ.* **2006**, *103*, 115–126.
16. Zhao, X.; Liang, S.L.; Liu, S.H.; Yuan, W.P.; Xiao, Z.Q.; Liu, Q.; Cheng, J.; Zhang, X.T.; Tang, H.R.; Zhang, X.; *et al.* The global land surface satellite (GLASS) remote sensing data processing system and products. *Remote Sens.* **2013**, *5*, 2436–2450.
17. Stisen, S.; Sandholt, I.; Norgaard, A.; Fensholt, R.; Eklundh, L. Estimation of diurnal air temperature using MSG SEVIRI data in West Africa. *Remote Sens. Environ.* **2007**, *110*, 262–274.
18. Tang, B.H.; Li, Z.-L. Estimation of instantaneous net surface longwave radiation from MODIS cloud-free data. *Remote Sens. Environ.* **2008**, *112*, 3482–3492.
19. Jacome, A.; Bernier, M.; Chokmani, K.; Gauthier, Y.; Poulin, J.; De Seve, D. Monitoring volumetric surface soil moisture content at the La Grande basin boreal wetland by radar multi polarization data. *Remote Sens.* **2013**, *5*, 4919–4941.
20. Wan, Z.M.; Li, Z.-L. Radiance-based validation of the V5 MODIS land-surface temperature product. *Int. J. Remote Sens.* **2008**, *29*, 5373–5395.
21. Jiang, G.M.; Li, Z.-L. Split-window algorithm for land surface temperature estimation from MSG1-SEVIRI data. *Int. J. Remote Sens.* **2008**, *29*, 6067–6074.
22. Wang, N.; Wu, H.; Nerry, F.; Li, C.R.; Li, Z.-L. Temperature and emissivity retrievals from hyperspectral thermal infrared data using linear spectral emissivity constraint. *IEEE Trans. Geosci. Remote Sens.* **2011**, *49*, 1291–1303.
23. Carlson, T.N.; Capehart, W.J.; Gillies, R.R. A new look at the simplified method for remote sensing of daily evapotranspiration. *Remote Sens. Environ.* **1995**, *54*, 161–167.
24. Jackson, R.; Hatfield, J.; Reginato, R.; Idso, S.; Pinter, P., Jr. Estimation of daily evapotranspiration from one time-of-day measurements. *Agr. Water Manage.* **1983**, *7*, 351–362.
25. Jiang, L.; Islam, S. A methodology for estimation of surface evapotranspiration over large areas using remote sensing observations. *Geophys. Res. Lett.* **1999**, *26*, 2773–2776.
26. Carlson, T. An overview of the "triangle method" for estimating surface evapotranspiration and soil moisture from satellite imagery. *Sensors* **2007**, *7*, 1612–1629.

27. Tang, R.L.; Li, Z.-L.; Tang, B.H. An application of the Ts-VI triangle method with enhanced edges determination for evapotranspiration estimation from MODIS data in arid and semi-arid regions: Implementation and validation. *Remote Sens. Environ.* **2010**, *114*, 540–551.
28. Wang, K.C.; Liang, S.L. An improved method for estimating global evapotranspiration based on satellite determination of surface net radiation, vegetation index, temperature, and soil moisture. *J. Hydrometeorol.* **2008**, *9*, 712–727.
29. Long, D.; Singh, V.P.; Scanlon, B.R. Deriving theoretical boundaries to address scale dependencies of triangle models for evapotranspiration estimation. *J. Geophys. Res.* **2012**, *117*, doi:10.1029/2011JD017079.
30. Tang, R.L.; Li, Z.-L.; Chen, K.-S.; Jia, Y.Y.; Li, C.R.; Sun, X.M. Spatial-scale effect on the SEBAL model for evapotranspiration estimation using remote sensing data. *Agric. For. Meteorol.* **2013**, *174*, 28–42.
31. Stisen, S.; Sandholt, I.; Norgaard, A.; Fensholt, R.; Jensen, K.H. Combining the triangle method with thermal inertia to estimate regional evapotranspiration—Applied to MSG-SEVIRI data in the Senegal River basin. *Remote Sens. Environ.* **2008**, *112*, 1242–1255.
32. Wang, K.C.; Li, Z.Q.; Cribb, M. Estimation of evaporative fraction from a combination of day and night land surface temperatures and NDVI: A new method to determine the Priestley-Taylor parameter. *Remote Sens. Environ.* **2006**, *102*, 293–305.
33. Anderson, M.C.; Norman, J.M.; Diak, G.R.; Kustas, W.P.; Mecikalski, J.R. A two-source time-integrated model for estimating surface fluxes using thermal infrared remote sensing. *Remote Sens. Environ.* **1997**, *60*, 195–216.
34. Norman, J.M.; Kustas, W.P.; Prueger, J.H.; Diak, G.R. Surface flux estimation using radiometric temperature: A dual temperature-difference method to minimize measurement errors. *Water Resour. Res.* **2000**, *36*, 2263–2274.
35. Zhao, W.; Li, Z.-L.; Wu, H.; Tang, B.H.; Zhang, X.Y.; Song, X.N.; Zhou, G.Q. Determination of bare surface soil moisture from combined temporal evolution of land surface temperature and net surface shortwave radiation. *Hydrol. Process.* **2013**, *27*, 2825–2833.
36. Zhao, W.; Li, Z.-L. Sensitivity study of soil moisture on the temporal evolution of surface temperature over bare surfaces. *Int. J. Remote Sens.* **2013**, *34*, 3314–3331.
37. Lu, J.; Tang, R.L.; Tang, H.J.; Li, Z.-L. A new parameterization scheme for estimating surface energy fluxes with continuous surface temperature, air temperature, and surface net radiation measurements. *Water Resour. Res.* **2014**, *50*, 1245–1259.
38. Lu, J.; Tang, R.L.; Tang, H.J.; Li, Z.-L. Derivation of daily evaporative fraction based on temporal variations in surface temperature, air temperature, and net radiation. *Remote Sens.* **2013**, *5*, 5369–5396.
39. Chehbouni, A.; Lo Seen, D.; Njoku, E.; Monteny, B. Examination of the difference between radiative and aerodynamic surface temperatures over sparsely vegetated surfaces. *Remote Sens. Environ.* **1996**, *58*, 177–186.
40. Lhomme, J.; Chehbouni, A.; Monteny, B. Sensible heat flux-radiometric surface temperature relationship over sparse vegetation: Parameterizing B^{-1}. *Bound. Lay. Meteorol.* **2000**, *97*, 431–457.
41. Gentine, P.; Entekhabi, D.; Polcher, J. The diurnal behavior of evaporative fraction in the soil-vegetation-atmospheric boundary layer continuum. *J. Hydrometeorol.* **2011**, *12*, 1530–1546.

42. Crago, R.D. Conservation and variability of the evaporative fraction during the daytime. *J. Hydrol.* **1996**, *180*, 173–194.
43. Trenberth, K.E.; Fasullo, J.T. Tracking earth's energy. *Science* **2010**, *328*, 316–317.
44. Li, Z.-L.; Tang, B.H.; Wu, H.; Ren, H.Z.; Yan, G.J.; Wan, Z.M. Satellite-derived land surface temperature: Current status and perspectives. *Remote Sens. Environ.* **2013**, *131*, 14–37.
45. Li, Z.-L.; Zhang, R.; Sun, X.; Su, H.; Tang, X.; Zhu, Z.; Sobrino, J. Experimental system for the study of the directional thermal emission of natural surfaces. *Int. J. Remote Sens.* **2004**, *25*, 195–204.
46. AmeriFlux Site and Data Exploration System. Available online: http://ameriflux.ornl.gov/ (accessed on 13 October 2013).
47. Suyker, A.E.; Verma, S.B. Interannual water vapor and energy exchange in an irrigated maize-based agroecosystem. *Agric. For. Meteorol.* **2008**, *148*, 417–427.
48. Tang, R.L.; Li, Z.-L.; Sun, X.M. Temporal upscaling of instantaneous evapotranspiration: An intercomparison of four methods using eddy covariance measurements and MODIS data. *Remote Sens. Environ.* **2013**, *138*, 102–118.
49. Twine, T.; Kustas, W.; Norman, J.; Cook, D.; Houser, P.; Meyers, T.; Prueger, J.; Starks, P.; Wesely, M. Correcting eddy-covariance flux underestimates over a grassland. *Agric. For. Meteorol.* **2000**, *103*, 279–300.
50. Quarmby, N.; Townshend, J.; Settle, J.; White, K.; Milnes, M.; Hindle, T.; Silleos, N. Linear mixture modelling applied to AVHRR data for crop area estimation. *Int. J. Remote Sens.* **1992**, *13*, 415–425.
51. Carlson, T.N.; Perry, E.M.; Schmugge, T.J. Remote estimation of soil moisture availability and fractional vegetation cover for agricultural fields. *Agric. For. Meteorol.* **1990**, *52*, 45–69.
52. Prihodko, L.; Goward, S.N. Estimation of air temperature from remotely sensed surface observations. *Remote Sens. Environ.* **1997**, *60*, 335–346.
53. Carlson, T.N.; Ripley, D.A. On the relation between NDVI, fractional vegetation cover, and leaf area index. *Remote Sens. Environ.* **1997**, *62*, 241–252.
54. Long, D.; Longuevergne, L.; Scanlon, B.R. Uncertainty in evapotranspiration from land surface modeling, remote sensing, and GRACE satellites. *Water Resour. Res.* **2014**, *50*, 1131–1151.
55. Kurc, S.A.; Small, E.E. Soil moisture variations and ecosystem-scale fluxes of water and carbon in semiarid grassland and shrubland. *Water Resour. Res.* **2007**, *43*, doi:10.1029/2006WR005011.